

Magnetic transition and magnetic structure of  $\text{Sr}_4\text{Ru}_3\text{O}_{10}$ Wei Bao,<sup>1</sup> Z.Q. Mao,<sup>2</sup> M. Zhou,<sup>2</sup> J. Hooper,<sup>2</sup> J.W. Lynn,<sup>3</sup> R.S. Freitas,<sup>4</sup> P. Schier,<sup>4</sup> Y. Liu,<sup>4</sup> H.Q. Yuan,<sup>5</sup> and M. Salamon<sup>5</sup><sup>1</sup>Los Alamos National Laboratory, Los Alamos, New Mexico 87545<sup>2</sup>Department of Physics, Tulane University, New Orleans, Louisiana 70118<sup>3</sup>NIST Center for Neutron Research, National Institute of Standards and Technology, Gaithersburg, Maryland 20899<sup>4</sup>Department of Physics, Pennsylvania State University, University Park, Pennsylvania 16802<sup>5</sup>Department of Physics, University of Illinois at Urbana-Champaign, Urbana, Illinois 61801

(Dated: March 23, 2024)

We have investigated the magnetic transition and magnetic structure of triple-layered ruthenate  $\text{Sr}_4\text{Ru}_3\text{O}_{10}$  directly using neutron scattering techniques. Only one ferromagnetic phase is observed, and previously proposed antiferromagnetic phase transitions are ruled out. The complex anisotropic magnetotransport, magnetization and in-plane metamagnetic behaviors of this quasi two-dimensional (2D) material are most likely due to magnetic domain processes with strong magnetocrystalline anisotropy and a strongly anisotropic demagnetization factor.

PACS numbers: 71.27.+a, 75.25.+z, 75.60.Ch, 75.30.Kz

Strontium ruthenates of the Ruddlesden-Popper (RP) series,  $\text{Sr}_{n+1}\text{Ru}_n\text{O}_{3n+1}$ , exhibit a rich variety of fascinating physical properties, such as unusual spin-triplet superconductivity in  $\text{Sr}_2\text{RuO}_4$  ( $n=1$ ) [1, 2, 3, 4], metamagnetic quantum criticality in  $\text{Sr}_3\text{Ru}_2\text{O}_7$  ( $n=2$ ) [5, 6, 7], and itinerant ferromagnetism in  $\text{SrRuO}_3$  ( $n=1$ ) [8, 9]. They have played a pivotal role in the past decade in the study of novel physics of strongly correlated electron systems.  $\text{Sr}_4\text{Ru}_3\text{O}_{10}$  is the  $n=3$  member of the RP series with triple layers of corner shared  $\text{RuO}_6$  octahedra separated by  $\text{SrO}$  rock-salt double layers. While  $\text{Sr}_2\text{RuO}_4$  and  $\text{Sr}_3\text{Ru}_2\text{O}_7$  are close to magnetic instabilities [10, 11, 12], bulk magnetization studies of  $\text{Sr}_4\text{Ru}_3\text{O}_{10}$  provide evidence for true long-range ferromagnetism with  $T_C = 105$  K [13, 14], lower than that seen in  $\text{SrRuO}_3$  ( $T_C = 160$  K) [8, 9]. The ferromagnetism in this material exhibits very unusual anisotropic properties under applied magnetic fields. Magnetization curves are distinctly different for magnetic fields applied along the  $c$  axis and in the basal plane, and an additional transition at  $T = 50$  K has been indicated [13, 14]. Below  $T$ , a metamagnetic transition is induced by a magnetic field applied in the plane. Very unusual transport properties, including ultrasharp magnetoresistivity steps and a non-metallic temperature dependence of resistivity, have been observed near this transition [15]. In addition, strong magnetoelastic coupling has been observed in this material [16].

It has been proposed that in  $\text{Sr}_4\text{Ru}_3\text{O}_{10}$  the Ru magnetic moments are canted; the  $c$ -axis components order in a ferromagnetic transition at  $T_C = 105$  K, while the in-plane components order in a separate antiferromagnetic transition at  $T = 50$  K [14, 16]. Within this picture, the metamagnetic transition is thought to be a transition from an antiferromagnetic to a ferromagnetic arrangement for the in-plane moment components. We have performed direct measurements of the magnetic structure in  $\text{Sr}_4\text{Ru}_3\text{O}_{10}$  by neutron scattering, which yields

a result that is inconsistent with this proposed magnetic picture. We find only a ferromagnetic transition at  $T_C = 100$  K with a normal order parameter and with an easy axis lying in the  $ab$  plane. This observation, together with magnetotransport and magnetization measurements, strongly suggests that the metamagnetic behavior for  $H // ab$  results from strong magnetocrystalline anisotropy and ferromagnetic domain formation. Our result clarifies the metamagnetic behavior in the ferromagnetic state of  $\text{Sr}_4\text{Ru}_3\text{O}_{10}$ , which has been a longstanding puzzle. This finding is of fundamental importance in understanding other novel properties in this class of materials [15, 16].

Single crystals of  $\text{Sr}_4\text{Ru}_3\text{O}_{10}$  used for this study were grown using a coating zone technique. The high quality of the crystals is indicated by the small residual resistivity in the 1.5–6.0  $\mu\Omega$  range [15]. The tiny orthorhombic distortion of the  $P6_{3mm}$  crystal structure [13] is negligible for this work, and we use the  $I4=mm$  tetragonal unit cell to label the reciprocal space with dimensions of  $a = b = 3.895$  and  $c = 28.46$  Å at 70 K. Samples used in this neutron scattering work at NIST are thin plates with the shortest dimension along the  $c$ -axis. A 0.1 g sample was oriented to investigate the  $(hhl)$  zone in reciprocal space and a 0.4 g sample for the  $(h0l)$  zone. A small amount of  $\text{SrRuO}_3$  intergrowth was observed in our experiments, which can be easily separated by its very different lattice parameter  $c = 7.86$  Å. Both triple-axis and two-axis modes of the thermal triple-axis spectrometer BT9 were used with neutrons of energy  $E = 14.7$  meV. The collimations were 40–48–44 in the two-axis mode, and 40–48–44–80 in the triple-axis mode. Pyrolytic graphite filters of 10 cm total thickness were used to reduce higher order neutrons. Sample temperature was regulated by a closed cycle refrigerator in zero field experiments, and by a 7 T superconducting cryomagnet in magnetic field experiments.

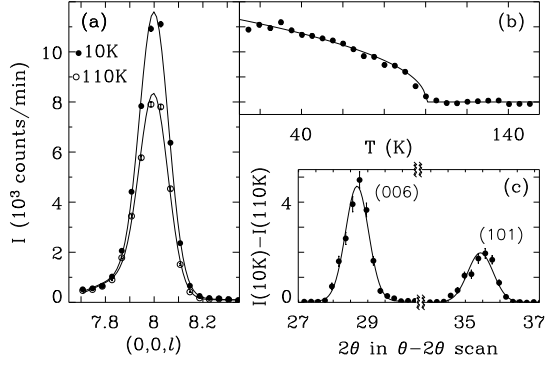


FIG. 1: Magnetic Bragg peaks coincide with structural Bragg peaks in  $\text{Sr}_4\text{Ru}_3\text{O}_{10}$ . (a) Scans along the interlayer direction through the (008) Bragg peak at 10 and 110 K. (b) Temperature dependence of the (008) Bragg peak, showing the magnetic transition at  $T_C = 100$  K. (c) Difference scans in the same unit as (a), representing magnetic Bragg intensities at (006) and (101).

Fig. 1(a) shows the (008) Bragg peak of  $\text{Sr}_4\text{Ru}_3\text{O}_{10}$  measured at 10 and 110 K. The enhanced intensity at low temperature is due to the magnetic transition at  $T_C = 100$  K. The resolution-limited peak width remains the same at low temperature and above  $T_C$ , indicating stacking of the  $\text{RuO}_6$  and  $\text{SrO}$  layers according to the crystal structure to form a macroscopic crystal, and a magnetic transition in the whole crystal. Scans, covering an area larger than a Brillouin zone, in both the (hhl) and (h0l) reciprocal zones, detected no additional temperature-dependent magnetic Bragg peaks, either commensurate or incommensurate. Hence, the magnetic structure in  $\text{Sr}_4\text{Ru}_3\text{O}_{10}$  follows the same symmetry of the crystal structure. Antiferromagnetic structures, such as layers of Ru moments stacking alternately along the c axis [16], are forbidden.

Fig. 1(b) shows the temperature dependence of the (008) Bragg peak, which serves as the squared magnetic order parameter of the phase transition. The order parameter behaves normally below  $T_C = 100$  K. In particular, it does not exhibit either extra enhancement at  $T = 50$  K as in the c-axis magnetization measurement, or a sharp drop below  $T_C$  as in the in-plane magnetization [13, 14]. Thus, the anomalies around 50 K in bulk magnetization measurements are not likely due to another magnetic transition in  $\text{Sr}_4\text{Ru}_3\text{O}_{10}$ , which is consistent with the fact that the specific heat of this material shows no anomaly at 50 K [17, 18].

Although the proposed antiferromagnetic arrangement is excluded by the selection rule for magnetic Bragg peaks, it is still interesting to investigate the magnetic order parameter under magnetic field. The 0.1 g sample was mounted in a cryomagnet with magnetic field along the [110] direction. Fig. 2 shows the (008) Bragg intensity at 5.8 K with magnetic field ramping up (solid

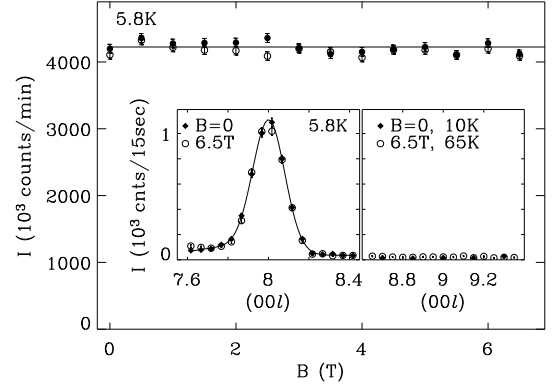


FIG. 2: Dependence of the (008) Bragg peak at 5.8 K on magnetic field applied along the in-plane [110] direction. The solid circles are for field ramping up, and open circles for ramping down. Inset: Scans through the allowed (008) or the forbidden (009) peak at  $B = 0$  (solid diamonds) and 6.5 T (open circles).

circles) and down (open circles). No first-order metamagnetic transition like that in the magnetization [14] was observed. The Bragg peak profile below and above  $B_C$  also remains the same, as shown for scans at 5.8 K for  $B = 0$  (solid symbols) and 6.5 T (open symbols) in the inset to Fig. 2. Similarly, no field effect can be detected in either the profile or intensity of the (008) Bragg peak at 18, 40 and 65 K. The magnetic field also does not induce extra intensity at forbidden peaks, such as (009), (see inset to Fig. 2).

The neutron scattering cross section from a magnetic structure is given by [19]

$$\langle q \rangle = \frac{n_0^2}{2} \langle f(q) \rangle^2 \left( \sum_{\mathbf{q}} \mathbf{q} \cdot \mathbf{q} \right) F(\mathbf{q}) F(\mathbf{q}); \quad (1)$$

where  $(n_0/2)^2 = 0.07265$  barns/ $\text{\AA}^3$ ,  $f(q)$  is the atomic form factor of the Ru ion [2, 10],  $\mathbf{q}$  the unit vector of  $q$ , and  $F(\mathbf{q})$  the  $l$ th Cartesian component of the magnetic structure factor per  $\text{Sr}_4\text{Ru}_3\text{O}_{10}$ . The factor  $(\sum_{\mathbf{q}} \mathbf{q} \cdot \mathbf{q})$  in Eq. (1) dictates that only magnetic moment components which are perpendicular to the neutron wave-vector transfer,  $q$ , contribute to magnetic neutron scattering. In particular, if the Ru magnetic moments actually pointed along the c-axis then the magnetic intensities would vanish at Bragg points (00l) where  $l$  is an even integer; thus magnetic intensity at peaks such as (008) in Fig. 1 and 2 rules out this proposed ferromagnetic structure [13, 14]. Furthermore, the field independent (008) Bragg intensity as shown in Fig. 2 rules out a canted magnetic structure with a c-axis component which rotates to the basal plane for  $B > B_C$  [16]. Instead, magnetic moments are aligned in the basal plane, and thus the rotation of the moments to the (110) direction when the field  $B > B_C$  would not change the neutron scattering cross section. This conclusion is consistent with the easy axis of the

related compound  $\text{SrRuO}_3$ , which lies in the basal plane [8, 20]. In addition, the demagnetization factor of the plate-like  $\text{Sr}_4\text{Ru}_3\text{O}_{10}$  samples also favors the in-plane orientation [21].

It is well known for ferromagnetic materials that the bulk magnetization does not directly reflect the magnetic order parameter due to domain formation when the magnetic field is below a certain strength [21]. Complex anisotropic behaviors in magnetic field can be induced by domain processes due to strong magnetocrystalline anisotropy, demagnetization factor, magnetostatic energy, magnetostriction and mutual interaction between the magnetization and the external field [21, 22]. For example,  $\text{SrRuO}_3$  has a very strong magnetocrystalline anisotropy. The internal crystalline anisotropy field is about 2T for the pseudo-cubic  $\text{SrRuO}_3$ , with easy axis along the [110] directions [8]. In the pseudo-tetragonal  $\text{SrRuO}_3$ , the easy axis lies along [100], while the c-axis is a direction of medium magnetization with the spin- $\uparrow$  field at 1.5 T [20]. Substantial magnetic field is required to line up magnetic moments of domains. Since the local environment for Ru in  $\text{Sr}_4\text{Ru}_3\text{O}_{10}$  is similar to that in  $\text{SrRuO}_3$ , it is not unrealistic to expect a similarly strong magnetocrystalline anisotropy in  $\text{Sr}_4\text{Ru}_3\text{O}_{10}$ , and complex magnetic behaviors can be understood within such a domain picture.

In Fig. 3, we present the magnetization loop for  $\text{Sr}_4\text{Ru}_3\text{O}_{10}$  for in-plane and out-of-plane field orientations. Consistent with the previously reported results [13, 14], the magnetization curve is extremely anisotropic. For  $H \parallel c$ , the remnant magnetization is almost equal to the saturated magnetization and the magnetization curve shows discontinuous jumps in the second and fourth quadrants, in sharp contrast with zero remnant magnetization for  $H \parallel ab$ . The out-of-plane field

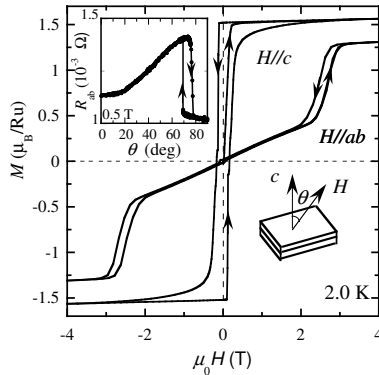


FIG. 3: Magnetization loop for  $\text{Sr}_4\text{Ru}_3\text{O}_{10}$  for in-plane and out-of-plane field orientations. Inset at lower right: schematic of field rotation with respect to the c-axis for the electrical transport measurement. Inset at upper left: the polar angle dependence of the in-plane resistance. All samples used in this work are from the same batch.

leads to behavior consistent with typical ferromagnets, and the larger magnetization is tempting for assigning the c-axis as the easy axis of magnetization. However, our neutron experiment demonstrates that the easy axis of  $\text{Sr}_4\text{Ru}_3\text{O}_{10}$  lies in the ab-plane. In addition, the in-plane field behavior is atypical for a ferromagnet and resembles a metamagnetic transition at 2.5 T. But our neutron scattering experiment (see Fig. 2) does not detect any increase in magnetic order parameter near 2.5 T. Thus, the metamagnetic behavior for  $H \parallel ab$  cannot be interpreted as the Stoner transition as in  $\text{Sr}_3\text{Ru}_2\text{O}_7$  [5, 6, 7].

Magnetic domains form in  $\text{Sr}_4\text{Ru}_3\text{O}_{10}$ , like in any sizeable ferromagnet. Cancellation of magnetization of domains with different in-plane easy axes is responsible for the low magnetization at low in-plane field, and a large field of 2.5 T is required to induce spin- $\uparrow$  and spin- $\downarrow$  in this material of strong magnetocrystalline anisotropy, as in  $\text{SrRuO}_3$  [22]. The energy barrier between the c-axis and an easy axis is likely much lower than that between two easy axes in the basal plane, which explains the easier alignment of moments along the c-axis. This domain picture is also consistent with the angular dependence of in-plane magnetoresistance of  $\text{Sr}_4\text{Ru}_3\text{O}_{10}$ , see insets in Fig. 3. When the 0.5 T applied field rotates from the ab-plane ( $\theta = 90^\circ$ ) toward the c-axis ( $\theta = 0^\circ$ ), the magnetoresistance exhibits a sharp jump at  $\theta \approx 20^\circ$  away from the ab-plane, indicating a first-order process in which the in-plane magnetization vectors of magnetic domains flip to the c-axis.

Now let us turn to the determination of microscopic magnetic structure of  $\text{Sr}_4\text{Ru}_3\text{O}_{10}$ . The same symmetry for the magnetic structure as the crystalline one requires ferromagnetic alignment of magnetic moments within a Ru layer. Thus the exchange interactions between moments within the plane should be ferromagnetic, instead of antiferromagnetic as suggested in the Ramani work [16]. The same symmetry requirement also dictates identical magnetic arrangements in every  $\text{RuO}_6$  triple-layer building block. With the moment oriented in the plane, what remains to be determined for the magnetic structure, then, is the relative magnitude and angle of magnetic moments in the three neighboring layers of a building block. The relation between magnetic moments in the two outer layers are further constrained by the symmetry. Therefore, the magnetic moments at the a site of the  $I4mm$  or  $P6mm$  space-group in the center plane and at the e sites of the two outer planes can be generally written as

$$M_{e1} = M_a [\cos(\phi) + \eta \sin(\phi)] \quad (2a)$$

$$M_a = M_a \quad (2b)$$

$$M_{e2} = M_a [\cos(\phi) - \eta \sin(\phi)]; \quad (2c)$$

where  $M_a$  is the moment size at the a site,  $\eta$  a number,  $\phi$  the angle between moments in the nearest neigh-

TABLE I: Magnetic Bragg cross-section,  $I_{\text{obs}}$ , observed at 10 K in bams per  $\text{Sr}_4\text{Ru}_3\text{O}_{10}$ . The theoretical cross-section,  $I_{\text{I}}$ , in the same units, is calculated for the collinear magnetic structure using  $\alpha = 0.44$ ,  $\beta = 0$  and  $M = 1.85(2) \text{ B/Ru}$  in Eq. (2).  $I_{\text{II}}$  is calculated for the non-collinear magnetic structure using  $\alpha = 0.60$ ,  $\beta = 29$  and  $M = 1.59(1) \text{ B/Ru}$  in Eq. (2).  $F_s^2$  is the squared structure factor for the crystal structure in bams per  $\text{Sr}_4\text{Ru}_3\text{O}_{10}$ .

$q$	$I_{\text{obs}}$	$I_{\text{I}}$	$I_{\text{II}}$	$F_s^2$
(0 0 2)	0.64(1)	0.66	0.65	1.564
(0 0 4)	0.11(4)	0.03	0.036	2.850
(0 0 6)	1.11(5)	1.33	1.36	10.85
(0 0 8)	1.69(8)	1.12	1.15	3.945
(0 0 10)	0.023(2)	0.022	0.022	0.207
(1 0 1)	1.06(6)	0.59	0.60	8.771
(1 0 3)	0.02(1)	0.014	0.015	1.294
(1 0 5)	3.2(4)	0.13	0.12	2.342
(1 0 7)	5(2)	0.66	0.68	195.1
(1 0 9)	0.06(2)	0.12	0.12	1.359
(1 1 2)	0.00(4)	0.08	0.08	1.927
(1 1 4)	0.00(5)	0.004	0.005	6.678

bor planes, and  $\mathbf{b}_1$  and  $\mathbf{b}_2$  are mutually perpendicular unit vectors in the basal plane. The average moment, as measured by a magnetometer, is  $M_{\text{ave}} = M [1 + 2 \cos(\beta)]/3$ , provided that the applied magnetic field does not alter

To determine the free parameters in Eq. (2), a set of magnetic Bragg intensities was measured. A couple of examples are shown in Fig. 1. The magnetic cross sections of  $\text{Sr}_4\text{Ru}_3\text{O}_{10}$  can be conveniently determined through the relation,

$$I_{\text{obs}}(q) = \frac{I(10\text{K}) - I(110\text{K})}{I(110\text{K})} F_s(q)^2; \quad (3)$$

where  $F_s(q)$  is the known structure factor per  $\text{Sr}_4\text{Ru}_3\text{O}_{10}$  of the structural Bragg peak at  $q$  [13]. These are listed in Table I. For (103), (105) and (107), the scattered neutron beam was nearly parallel to the sample plate, and the measured  $I(110\text{K})$  cannot be properly accounted for by the squared structure factor  $F_s^2$  due to extinction/absorption. Therefore,  $I_{\text{obs}}$  for them in Table I are not reliable. Among the remaining Bragg peaks, (002), (006), (008), (0,0,10) and (101) gain more than 10% intensity at low temperature due to the ferromagnetic transition.

The simplest magnetic structure consistent with Eq. (2) is the one with identical magnetic moments for the Ru ions, namely,  $(\alpha; \beta) = (1; 0)$  in Eq. (2), or  $M_{e1} = M_a = M_{e2}$ . For this magnetic structure, Eq. (1) is reduced to

$$I(q) = \frac{F_x(q)^2}{2} \frac{1 + \cos^2(\theta)}{2} F_x(q)^2; \quad (4)$$

where  $\theta$  is the angle between  $q$  and the  $c$  axis, and equal populations of magnetic domains are assumed for the

zero field experiments. However, Eq. (4) does not provide a good description of the measured  $I_{\text{obs}}$ . The  $I_{\text{obs}}^2$  can be reduced by a order of magnitude in a least-squares fit of  $I_{\text{obs}}$  to Eq. (1) with unrestricted  $\alpha$  and  $\beta$  for the magnetic model in Eq. (2). Both  $(\alpha; \beta)_{\text{I}} = (0.44; 0)$  and  $(0.6, 29)_{\text{II}}$  with  $\chi^2/21$  best fit the data, and an arc connecting them in the  $\alpha$ - $\beta$  plane is a slightly inferior fit. Hence, there is no unique result. In Table I we present theoretical cross sections  $I_{\text{I}}$  for the collinear magnetic structure  $(\alpha; \beta) = (0.44; 0)$  with  $M = 1.85(2) \text{ B/Ru}$ , and  $I_{\text{II}}$  for the non-collinear structure  $(0.6, 29)$  with  $M = 1.59(1) \text{ B/Ru}$ . Using a subset of  $I_{\text{obs}}$  in Table I with  $I(10\text{K})/I(110\text{K}) > 1.1$ , or including data of larger uncertainty in the least-square fit does not affect the results. The average moments of the two magnetic models are  $M_{\text{ave}} = 1.2$  and  $1.1 \text{ B/Ru}$  respectively, both comparable to the experimental value shown in Fig. 3.

In summary, we found only one magnetic transition at 100 K with easy axis in the basal plane for  $\text{Sr}_4\text{Ru}_3\text{O}_{10}$ . No additional antiferromagnetic transitions are observed. Our experiments strongly suggest that the complex magnetotransport, magnetization and metamagnetic behaviors results from magnetic domain processes in this quasi 2D material of strong magnetic crystalline anisotropy.

Work at LANL were supported by US DOE, at Tulane by the Louisiana Board of Regents support fund LEQSF (2003-06)-RD-A-26 and pilot fund NSF/LEQSF (2005)-p fund-23 and a grant from Research Corporation.

- 
- [1] K. Ishida et al, Nature 396, 658 (1998).
  - [2] J. A. Du y et al, Phys. Rev. Lett. 85, 5412 (2000).
  - [3] A. P. M. ackenzie and Y. M. aeno, Rev. Mod. Phys. 75, 657 (2003).
  - [4] K. D. Nelson et al, Science 306, 1151 (2004).
  - [5] R. S. Perry et al, Phys. Rev. Lett. 86, 2661 (2001).
  - [6] S. A. G rigera et al, Science 294, 329 (2001).
  - [7] S. A. G rigera et al, Science 306, 1154 (2004).
  - [8] A. K anbayasi, J. Phys. Soc. Japan 41, 1876 (1976).
  - [9] P. A llen et al, Phys. Rev. B 53, 4393 (1996).
  - [10] Y. Sidis et al, Phys. Rev. Lett. 83, 3320 (1999).
  - [11] D. J. Singh and I. I. M azin, Phys. Rev. B 63, 165101 (2001).
  - [12] L. Capogna, Phys. Rev. B 67, 12504 (2003).
  - [13] M. K. C rawford et al, Phys. Rev. B 65, 214412 (2002).
  - [14] G. C ao et al, Phys. Rev. B 68, 174409 (2003).
  - [15] Z. Q. M ao et al, Phys. Rev. Lett. 96, 077205 (2006).
  - [16] R. Gupta et al, Phys. Rev. Lett. 96, 067004 (2006).
  - [17] X. N. Lin et al, Solid State Comm. 130, 151 (2004).
  - [18] Y. J. Jo et al, cond-mat/0605504.
  - [19] G. L. Squires, Introduction to the Theory of Thermal Neutron Scattering (Cambridge University Press, Cambridge, 1978).
  - [20] A. K anbayasi, J. Phys. Soc. Japan 41, 1879 (1976).
  - [21] A. H. M orrison, The Physical Principles of Magnetism (John Wiley & Sons, Inc., New York, 1965), ch. 6{7.

[22] A .K anbayasi, J.P hys. Soc. Japan 44, 89 (1978) .